Please cite this article in press as: Zhang et al., Role of the Internal Limiting Membrane in Structural Engraftment and Topographic Spacing of Transplanted Human Stem Cell-Derived Retinal Ganglion Cells, Stem Cell Reports (2020), https://doi.org/10.1016/j.stemcr.2020.12.001

Stem Cell Reports
Article
ISSCR
OPEN ACCESS

Role of the Internal Limiting Membrane in Structural Engraftment and Topographic Spacing of Transplanted Human Stem Cell-Derived Retinal Ganglion Cells

Kevin Y. Zhang,[1,3] Caitlyn Tuffy,[1,3] Joseph L. Mertz,[1] Sarah Quillen,[1] Laurence Wechsler,[1] Harry A. Quigley,[1] Donald J. Zack,[1,2] and Thomas V. Johnson[1,4,*]

[1]Glaucoma Center of Excellence, Wilmer Eye Institute, Johns Hopkins University School of Medicine, 600 North Wolfe Street, Maumenee B-110, Baltimore, MD 21287, USA

[2]Departments of Molecular Biology and Genetics, Neuroscience, and Genetic Medicine, Johns Hopkins University School of Medicine, Baltimore, MD 21287, USA

[3]These authors contributed equally

[4]Lead Contact

*Correspondence: johnson@jhmi.edu

https://doi.org/10.1016/j.stemcr.2020.12.001

SUMMARY

Retinal ganglion cell (RGC) replacement holds potential for restoring vision lost to optic neuropathy. Transplanted RGCs must undergo neuroretinal integration to receive afferent visual signals for processing and efferent transmission. To date, retinal integration following RGC transplantation has been limited. We sought to overcome key barriers to transplanted human stem cell-derived RGC integration. Following co-culture *ex vivo* on organotypic mouse retinal explants, human RGCs cluster and extend bundled neurites that remain superficial to the neuroretina, hindering afferent synaptogenesis. To enhance integration, we increased the cellular permeability of the internal limiting membrane (ILM). Extracellular matrix digestion using proteolytic enzymes achieved ILM disruption while minimizing retinal toxicity and preserving glial reactivity. ILM disruption is associated with dispersion rather than clustering of co-cultured RGC bodies and neurites, and increased parenchymal neurite ingrowth. The ILM represents a significant obstacle to transplanted RGC connectivity and its circumvention may be necessary for functional RGC replacement.

INTRODUCTION

Retinal ganglion cell (RGC) replacement provides a possible therapeutic strategy to reverse vision loss from optic neuropathies such as glaucoma, the world's leading cause of irreversible blindness (Quigley and Broman, 2006; Tham et al., 2014). Promising photoreceptor transplantation studies (Barber et al., 2013; MacLaren et al., 2006; Pearson et al., 2012; Singh et al., 2013), including human-rodent xenografts (Barnea-Cramer et al., 2016; Gagliardi et al., 2018; Gonzalez-Cordero et al., 2017; Lin et al., 2018; Zou et al., 2019), provide proof of principle that vision restoration may be attainable by mammalian retinal cell replacement. However, unlike photoreceptors, RGCs are projection neurons and their functional replacement requires bidirectional visual pathway integration. Studies of endogenous RGC axon regeneration following injury identify numerous molecular pathways that can be targeted to drive optic nerve regeneration and efferent visual signal propagation by exogenous transplanted RGCs (Li et al., 2017; Lim et al., 2016; Moore et al., 2009; Park et al., 2008; Wang et al., 2020; Yin et al., 2006). However, factors limiting transplanted RGC somal migration, spatial patterning, and dendrite integration within the recipient mammalian retina, all of which are necessary for achieving afferent input, are equally important to functional vision restoration and remain comparatively understudied.

A number of groups have transplanted various neural progenitors and RGC precursor cell types into rodent eyes with generally low survival and without clear evidence of functional RGC replacement (Becker et al., 2016; Chao et al., 2017; Cho et al., 2012; Divya et al., 2017; Hertz et al., 2014; Singhal et al., 2012; Singhal et al., 2008; Wang et al., 2019; Wu et al., 2018). Human embryonic stem (hES) cell-derived RGCs transplanted into rat eyes have been reported to localize to the RGC layer (RGCL), although these cells did not extend neurites and did not express RNA binding protein with multiple splicing (RBPMS) (Zhang et al., 2020). Recently, a pivotal study yielded qualified success in transplanting primary mouse RGCs into rat recipients, documenting relatively rare instances of mature RGC morphology, structural synaptogenesis, and functional electrophysiologic responses to light in spite of poor survival (Venugopalan et al., 2016). Although encouraging, progression from these initial studies to functional and clinically relevant RGC transplantation requires significantly increasing the efficiency of retinal integration of transplanted neurons, a goal that would be aided by better understanding the key barriers that impede integration.

Gene therapy studies suggest that the internal limiting membrane (ILM) is a major barrier to retinal neuronal

Please cite this article in press as: Zhang et al., Role of the Internal Limiting Membrane in Structural Engraftment and Topographic Spacing of Transplanted Human Stem Cell-Derived Retinal Ganglion Cells, Stem Cell Reports (2020), https://doi.org/10.1016/j.stemcr.2020.12.001

transduction by intravitreally administered viral vectors (Boye et al., 2016; Dalkara et al., 2009; Takahashi et al., 2017; Teo et al., 2018). The ILM is a basement membrane composed of extracellular matrix (ECM) proteins including laminin, collagen IV, perlecan, nidogen, and others (Halfter et al., 2014). Cellular interactions with the ILM play important developmental roles in retinal patterning of neurons, glia, and blood vessels (Clements et al., 2017; Edwards et al., 2010, 2011; Riccomagno et al., 2014). The outer limiting membrane, which is not a true basement membrane but rather a cellular structure composed of adherens junctions between Müller glia and photoreceptor plasma membranes, impedes integration of subretinally transplanted photoreceptors (Barber et al., 2013; West et al., 2008). Some have speculated that the ILM might impede retinal integration of RGCs following intravitreal transplantation (Kurimoto et al., 2001; Miltner and La Torre, 2019; Nishida et al., 2000; Peynshaert et al., 2019; Young et al., 2000); however, empiric data to support this conjecture are lacking. In prior work, we directly evaluated the ILM's impact on intraretinal migration of mesenchymal stem cells (MSCs) but found that reactive gliosis, rather than the ILM, impedes engraftment of that particular cell type (Johnson et al., 2010). To our knowledge, the role of the ILM in engraftment of transplanted neurons, including RGCs, has not been directly investigated.

During development, spatial localization of RGCs into a tiled mosaic is important for retinotopic patterning. RGC localization ultimately results from coordinated cell differentiation, migration, and selective apoptosis to achieve non-overlapping dendritic fields of similar RGC subtypes (Beros et al., 2018; Icha et al., 2016; McCabe et al., 1999; Riccomagno et al., 2014; Upton et al., 2007). RGC interactions with the ILM are important for normal spatial patterning (Clements et al., 2017; Riccomagno et al., 2014). Given modest success of RGC transplantation thus far, it remains unclear whether and how transplanted RGCs might spread to cover the retina. Developing methodologies for characterizing spatial localization patterns of transplanted RGCs in a formal quantitative manner is key to ensuring coverage that recapitulates functional retinotopic maps.

Since rodent and primate RGC physiologies are driven by fundamentally divergent gene expression profiles (Peng et al., 2019), studying human RGC transplantation is critical to clinical translation. Several laboratories have developed methods for generating RGCs from human stem cells (Lee et al., 2018; Sluch et al., 2017; Teotia et al., 2017). Previously, we genome engineered hES cells to express fluorescent reporters under control of the *BRN3B* gene. We optimized a soluble factor-based differentiation protocol to efficiently produce and immunopurify RGCs, and we reported their transcriptomic and electrophysiological characteristics (henceforth referred to as hES-RGCs) (Daniszewski et al., 2018; Sluch et al., 2015, 2017).

Herein, we examine the survival and morphology of hES-RGCs following co-culture *ex vivo* on adult murine organotypic retinal explants to characterize their potential for spontaneous retinal engraftment. We and others have previously published extensive characterizations of this model that include assessments of retinal cell type-specific survival and expression patterns, glial reactivity, and electrophysiology over time for up to 14 days in culture (Alarautalahti et al., 2019; Bull et al., 2011; Johnson et al., 2010, 2016; Johnson and Martin, 2008). The progressive degeneration of endogenous RGCs that follows the axotomy necessary to explant the retina is a strength, in that it models the pathologic context in which RGC transplantation is most relevant: severe optic neuropathy. Retinal explants exclude MSCs from engraftment in a manner similar to that observed after injection into the living eye (Johnson et al., 2010). Using this model and combining robust topographical spatial analyses with high-resolution three-dimensional (3D) confocal microscopy image reconstruction techniques not previously applied to retinal neuronal transplantation, we provide the first direct evidence that the ILM plays a central role in hES-RGC topographic spacing and in obstructing neurite localization to the retinal parenchyma following exogenous application.

RESULTS

Survival and Topographic Localization of Transplanted hES-RGCs

We applied hES-RGCs in a 5-μL single-cell suspension at three doses (1.55×10^4, 2.5×10^4, or 5.0×10^4 cells/retina) onto the inner surface of adult mouse organotypic retinal explants. Following 1 week of co-culture, 12.6% ± 8.2% of transplanted hES-RGCs survived (average of the three doses). The lowest transplantation dose exhibited the lowest survival rate (Figure 1A). Microscopic evaluation of retinal tissue as a flat mount permitted examination of the two-dimensional spatial arrangement of surviving hES-RGCs and their neurites (Figures 1B–1F). Predominantly, hES-RGC somas concentrated within clusters with direct contact between adjacent cell bodies. Outside of clusters were sizable spaces devoid of hES-RGC somas. We identified relatively few dispersed single cells. Individual neurites and compacted linear neurite bundles extended from cell clusters (on average 6.8 bundles/100 hES-RGCs). Neurites possessed terminal structures resembling growth cones.

We quantified the topographic spatial clustering of co-cultured hES-RGCs on retinal explants and compared this with endogenous RGCs immunolabeled for RBPMS on separate retinal explants without hES-RGCs (Figure 1M).

Please cite this article in press as: Zhang et al., Role of the Internal Limiting Membrane in Structural Engraftment and Topographic Spacing of Transplanted Human Stem Cell-Derived Retinal Ganglion Cells, Stem Cell Reports (2020), https://doi.org/10.1016/j.stemcr.2020.12.001

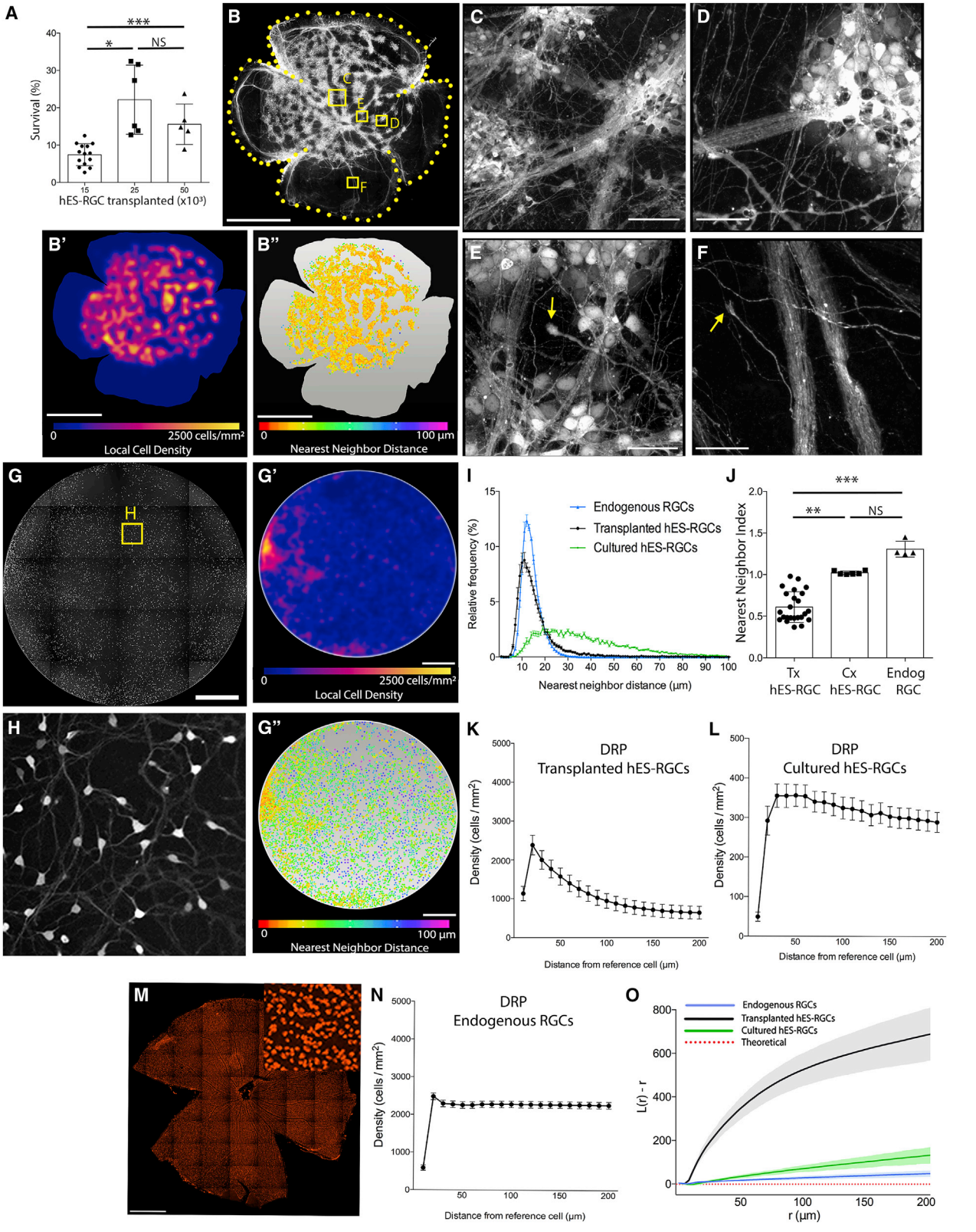

(legend on next page)

The overall average density of co-cultured hES-RGCs was 253.9 ± 243.3 cell/mm^2 covering 38.8% ± 11.0% of the retinal surface area. The hES-RGC density within clusters, however, was 2,587.5 ± 1,394.2 cell/mm^2, similar to the overall density of endogenous RGCs (2,332.8 ± 263.7 cell/mm^2). The average hES-RGC nearest neighbor distance (NND) was 16.8 ± 4.5 μm (Figure 1I), similar to what we and others (Davis et al., 2016; Jones et al., 2019) measured for endogenous RGCs (13.5 ± 0.5 μm, Figure 1I). The nearest neighbor index (NNI) normalizes the NND to theoretical conditions of complete spatial randomness (CSR) and measured 0.6 ± 0.2 in transplanted hES-RGCs, indicating cell clustering given a value <1 (Clark and Evans, 1954). By comparison, NNI was 1.3 ± 0.1 for endogenous RGCs (Figure 1J). Density recovery profiles (DRPs), representing the average local spatial density of neighboring RGCs as a function of distance from each index RGC, demonstrated an expected peak followed by plateau for endogenous RGCs (Figure 1N), indicating spatial regularity. In contrast, hES-RGC DRPs demonstrated a rapid exponential decline following the peak (Figure 1K), indicating cell clustering. L(r)-r describes the DRP's deviation from CSR to objectively compare spatial clustering between experimental groups, which is indicated by a positive deviation from zero. L(r)-r for co-cultured hES-RGCs rose steeply over CSR at short distances, whereas endogenous RGCs were only modestly more clustered than CSR (Figure 1O). Across multiple experiments, we co-cultured freshly isolated hES-RGCs or thawed cryopreserved hES-RGCs and noted no systematic differences in cell survival or clustering when applied to retinal explants (data not shown).

For comparison, we evaluated spacing of freshly isolated hES-RGCs plated at 250 cells/mm^2 on poly-L-ornithine and laminin-coated polystyrene. After 1 week, hES-RGC survival was significantly greater than when cultured on retinal explants (81.6% ± 12.7%, $p < 0.001$). hES-RGCs in cell culture elaborated long neurite processes intertwined in a complex lattice, but we identified no compact neurite bundles (Figures 1G and 1H). Cell somas were evenly dispersed, with only occasional clusters at the well periphery and very little inter-somal contact (Figure 1G). The average NND was 38.5 ± 2.6 μm (Figure 1I). The NNI was 1.03 ± 0.02, indicative of CSR (Figure 1J). The DRP demonstrated a modest, gradual decline after peaking at 30 μm, indicating minimal clustering (Figure 1L), and L(r)-r showed significantly less clustering than when hES-RGCs were transplanted onto retinal explants (Figure 1O). We performed a similar analysis using thawed cryopreserved hES-RGCs, which similarly failed to demonstrate significant soma or neurite clustering, but rather exhibited metrics consistent with spatial regularity (Figure S1).

In sum, hES-RGCs exhibited lower survival, compact bundling of long neurites, and clustering of hES-RGC somas when cultured on organotypic retinal explants as compared with poly-L-ornithine and laminin-coated polystyrene. Therefore, local intrinsic retinal factors may impair survival and induce cell body and neurite clustering after transplantation.

Spontaneous Structural Engraftment of Transplanted hES-RGC Neurites

We next examined the 3D structural arrangement of co-cultured hES-RGCs and their neurites in relation to the recipient neuroretina. Tracking individual processes within the neurite network extending from hES-RGCs clusters was not feasible in sectioned tissue because neurites entered and exited the plane of section. We therefore acquired confocal microscopic z stacks of retinal flat mounts for volumetric analysis (Figures 2A and 2D). Away from cut tissue edges, hES-RGC localization within the recipient retina was negligible; nearly all hES-RGC somas and neurites remained in a transplanted cell layer distinctly superficial to the RGCL (Figure S2A and Video S1). Cryosections confirmed that, away from cut edges, hES-RGC somas and neurites were not present within the retinal parenchyma (Figures 2B and 2C).

In contrast, near cut edges of the retinal explant, hES-RGCs infiltrated all retinal layers (Figures 2D–2F, Video S2). Precise quantification of hES-RGC localization to individual retinal layers was not feasible due to local disruption of the laminar architecture near cut edges. Intraretinal hES-RGC soma and neurite density was greatest near the edges

Figure 1. Topographic Spacing of hES-RGCs in Following Co-culture on Neural Retina

hES-RGCs were co-cultured (simulating transplantation [Tx]) onto the surface of organotypic retinal explants or cultured (Cx) on poly-L-ornithine and laminin coated for 1 week. RGC survival was lower when fewer cells were transplanted (A). Epifluorescence microscopy revealed the morphology and spacing of tdTomato$^+$ hES-RGCs cultured on retinal explants (B–F) vs on laminin-coated polystyrene (G, H). Arrows point to growth cone-like structures. Heat maps (B′, G′) show local cell density and NND maps (B″, G″) show the distance between each cell and its nearest neighbor, which is also plotted as a histogram (I). Nearest neighbor index (J) normalizes the mean NND to conditions of complete spatial randomness (CSR); values < 1.0 indicate clustering. Density recovery profiles (DRP, K, L, N) demonstrate the mean RGC density as a function of distance from each RGC in the sample. Ripley's L function (O) normalizes the DRP to theoretical CSR conditions such that positive deviations from zero indicate clustering (shaded areas indicate 95% confidence interval). Comparisons with RBPMS-expressing endogenous RGCs in adult C57BL/6 mouse retina are shown (M). Scalebars: 1.25 mm (B, G, M); 50 μm (C–F). Error bars: SD (A, J); SEM (I, K, L, N). *$p \leq 0.05$, **$p \leq 0.01$, ***$p \leq 0.001$, NS: $p > 0.05$.

Please cite this article in press as: Zhang et al., Role of the Internal Limiting Membrane in Structural Engraftment and Topographic Spacing of Transplanted Human Stem Cell-Derived Retinal Ganglion Cells, Stem Cell Reports (2020), https://doi.org/10.1016/j.stemcr.2020.12.001

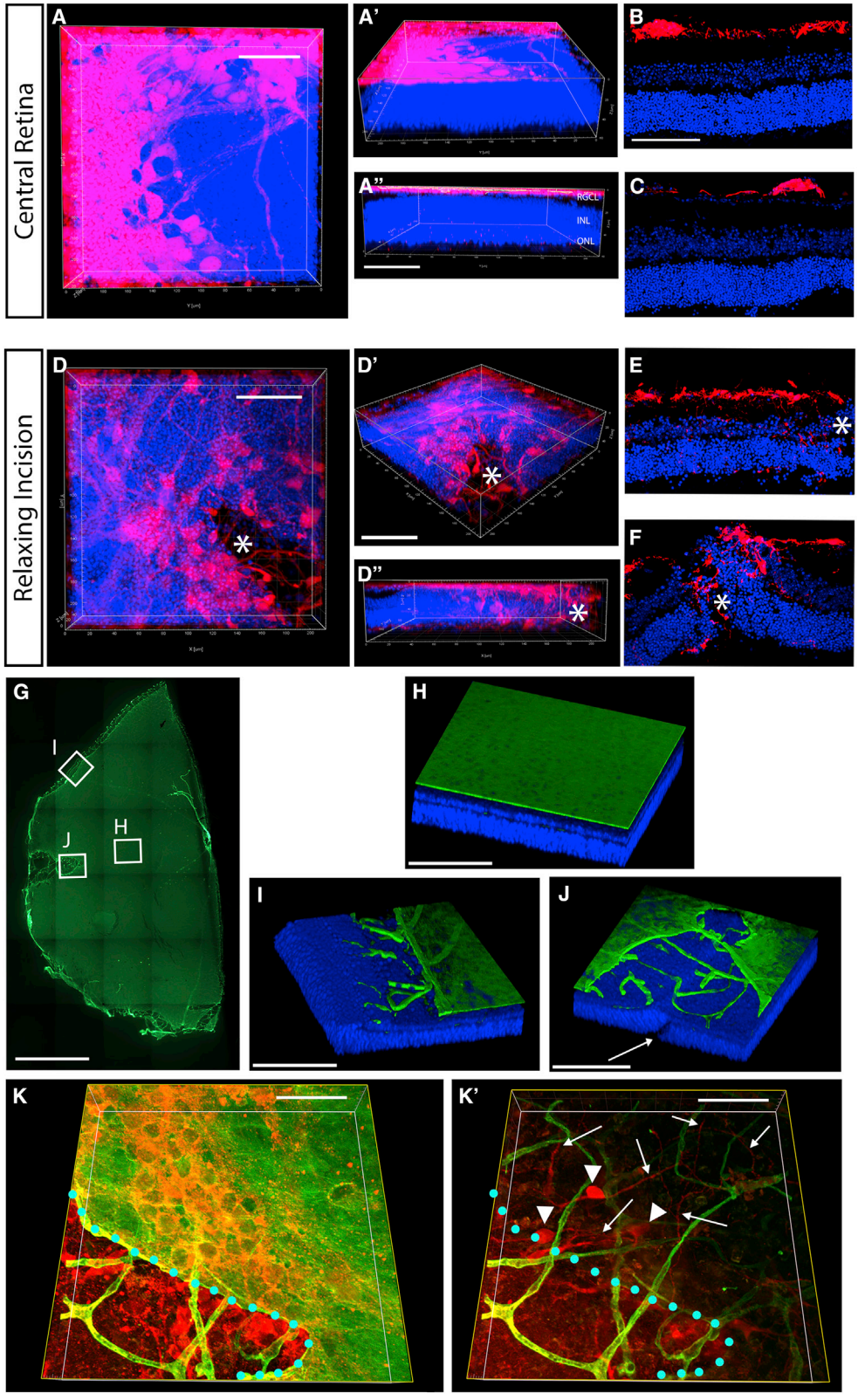

(legend on next page)

Please cite this article in press as: Zhang et al., Role of the Internal Limiting Membrane in Structural Engraftment and Topographic Spacing of Transplanted Human Stem Cell-Derived Retinal Ganglion Cells, Stem Cell Reports (2020), https://doi.org/10.1016/j.stemcr.2020.12.001

and decreased with distance from the edge. This pattern was consistent with neurite entry from the retinal tissue edge and lateral intraretinal migration, which suggested that a barrier to hES-RGC retinal ingrowth exists at a location superficial to the RGCL, where the ILM is positioned.

We hypothesized that the ILM obstructs structural ingress of co-cultured hES-RGCs. Examination of flat-mounted retinal explants confirmed homogeneous ILM integrity in central flat mounts. However, near cut edges, the ILM was abruptly broken and neural retina containing laminin^{+} vasculature was exposed deep to retracted ILM (Figures 2G–2J). Indeed, hES-RGC somas and neurites were identified deep to the ILM only in areas directly adjacent to retinal explant edges where the ILM was mechanically disrupted (Figure 2K).

ILM Disruption by Enzymatic Digestion

In order to increase cellular permeability of the ILM, we evaluated enzymatic methods of ECM digestion in retinal explants. We sought to identify an approach that strongly disrupts structural proteins at the ILM while minimizing off-target toxicity to inner retinal neurons and glia, so that the effect of enzymes could be attributed specifically to its disruptioon of the ECM.

We tested several proteolytic enzymes, applied at multiple concentrations directly onto the retinal explant ILM surface, and then inactivated them with ovalbumin and bovine serum albumin prior to washout. Histologic assessments at multiple timepoints included (1) the presence of ILM-associated protein immunoreactivity measured as a linear distance over the explant surface, and (2) a qualitative masked grading scale characterizing regularity and gaps in immunoreactivity (Figure S3). In control basic salt saline (BSS)-treated retinal explants, laminin and collagen IV were present as a continuous band at the ILM that persisted unchanged through 11 days of culture. Both proteins were initially expressed within the retinal vasculature, although this diminished with time in culture (Figures 3A–3C, 3E, and S2). Papain (10–45 U/mL) and pronase E at the highest dose tested (3 U/mL) eliminated laminin immunoreactivity at the ILM within hours, but laminin remained relatively preserved in retinal blood vessels and weakly in a few RGCL and inner nuclear layer (INL) cells, suggesting spatial restriction of enzymatic activity (Figures 3A and 3E). In contrast, collagenase (20–30 U/mL) and lower-dose pronase E (0.6 U/mL) caused subtle irregularity and discontinuity of laminin immunoreactivity at the ILM at day 0 (Figures 3A and 3E), and marked disruption by day 7 (Figures 3A, 3B, 3E, and S2).

Papain rapidly digested collagen IV at the ILM, whereas collagenase and both doses of pronase E caused irregularity and focal disruption of collagen IV staining at day 0 that were less extensive than those observed for laminin. After 7–11 days in culture, papain and pronase E (3 U/mL) produced greater disruption in collagen IV reactivity at the ILM than collagenase or lower-dose pronase E (Figures 3C, 3E, and S2).

Alpha-dystroglycan is a membrane-associated protein, localized to Müller cells at the ILM, that is important for cellular binding and signaling with ECM proteins, including laminin (Clements et al., 2017). Alpha-dystroglycan immunoreactivity was strong at the ILM but more granular in appearance than laminin or collagen IV in control retinal explants (Figures 3D and S2). Papain, collagenase, and pronase E (3 U/mL) were associated with early and persistent decreases in alpha-dystroglycan immunoreactivity at the ILM. However, following pronase E (0.6 U/mL) treatment, alpha-dystroglycan immunoreactivity remained similar to control throughout the culture period (Figures 3D and S2).

ILM degradation by proteolytic enzymes was confirmed by transmission electron microscopy. In BSS-treated retina, the ILM was a continuous electron-dense linear membrane external to Müller cell footplates. Fibrillar deposits from adherent posterior vitreous cortex overlaid the ILM (Figure 3F). Papain, collagenase, and pronase (3 U/mL) resulted in complete ILM loss, and also considerable degenerative changes to inner retinal Müller cells, astrocytes, and RGC axons (Figure S4). In contrast, pronase (0.6 U/mL) produced areas of near-complete ILM loss juxtaposed with

Figure 2. Structural Ingrowth of Co-cultured RGCs Is Greater Near Sites of Physical Retinal and ILM Disruption

Three-dimensional reconstructions of confocal microscopy z stacks are shown (A, D, G–K). Co-cultured hES-RGCs (red) extended neurites that remained superficial to the neural retina when located centrally in the retinal explant (A–C). Near retinal explant edges or sites of relaxing incisions, hES-RGC cell bodies and neurites migrated into the neural retina (D–F). Cryosections from separate retinal explants are shown (B, C, E, F). Asterisks indicate sites of retinal disruption (D–F). Immunohistochemistry for laminin (green) shows intact and continuous ILM in the central retina, with discontinuity at the edges and at relaxing incisions (G–J). Nuclei are labeled with DAPI (blue). Higher-magnification images (H–J) demonstrate that underlying retina and retinal vasculature are exposed at peripheral areas of mechanical ILM disruption. (J) Arrow highlights retinal discontinuity caused by a relaxing incision. Near areas of ILM discontinuity, hES-RGC cell bodies migrate laterally underneath the ILM and extend neurites laterally through the retinal tissue. K and K′ show a 3D reconstructed block of retinal tissue viewed from the top down. K′ is the same block with the most superficial confocal slices that include the ILM removed to reveal the underlying vasculature and hES-RGCs. The edge of the ILM is marked in teal dots. Arrowheads point to hES-RGC somas and arrows point to hES-RGC neurites. Scalebars: 1.25 mm (G); 50 μm (A,B,D,H–K).

Please cite this article in press as: Zhang et al., Role of the Internal Limiting Membrane in Structural Engraftment and Topographic Spacing of Transplanted Human Stem Cell-Derived Retinal Ganglion Cells, Stem Cell Reports (2020), https://doi.org/10.1016/j.stemcr.2020.12.001

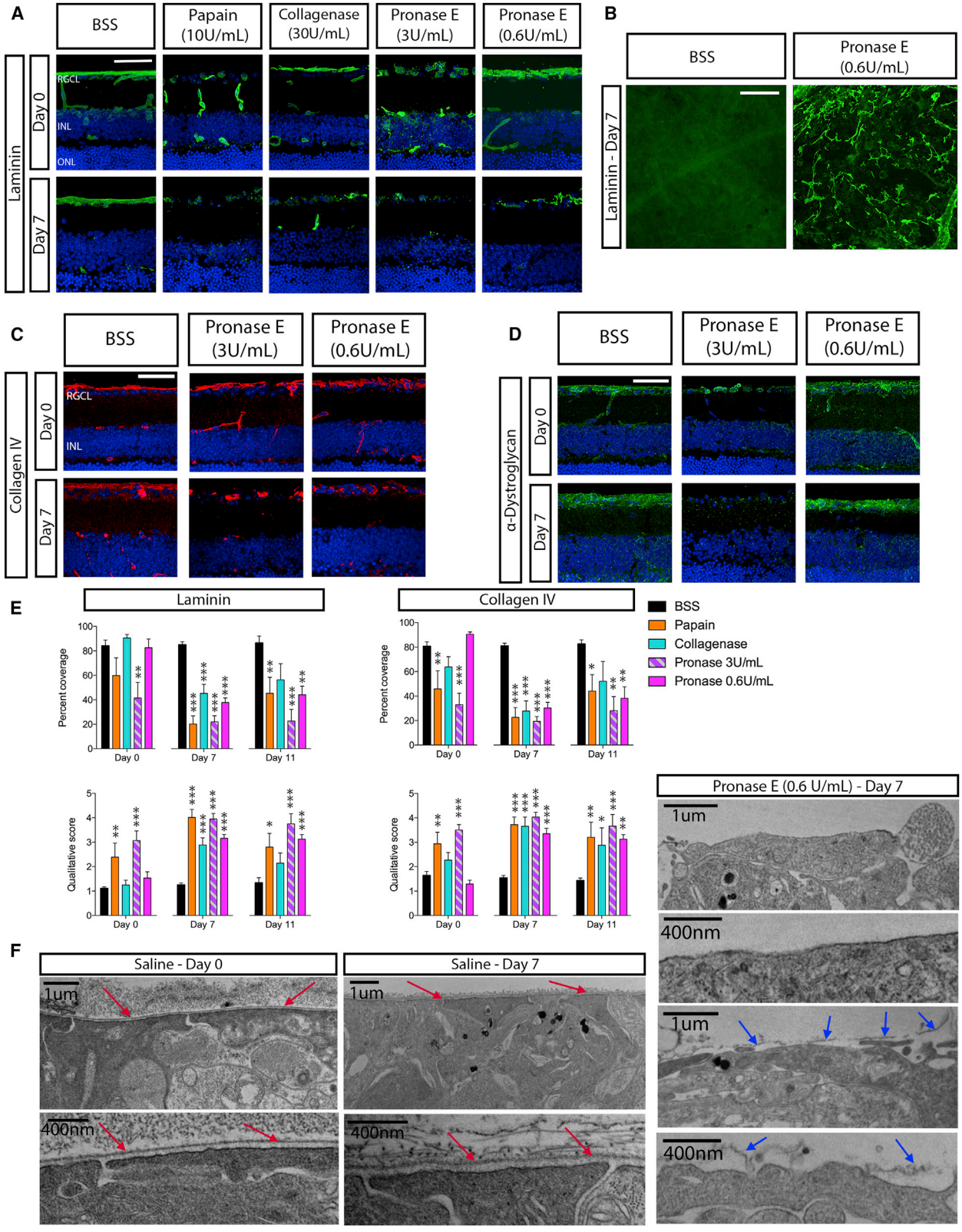

(legend on next page)

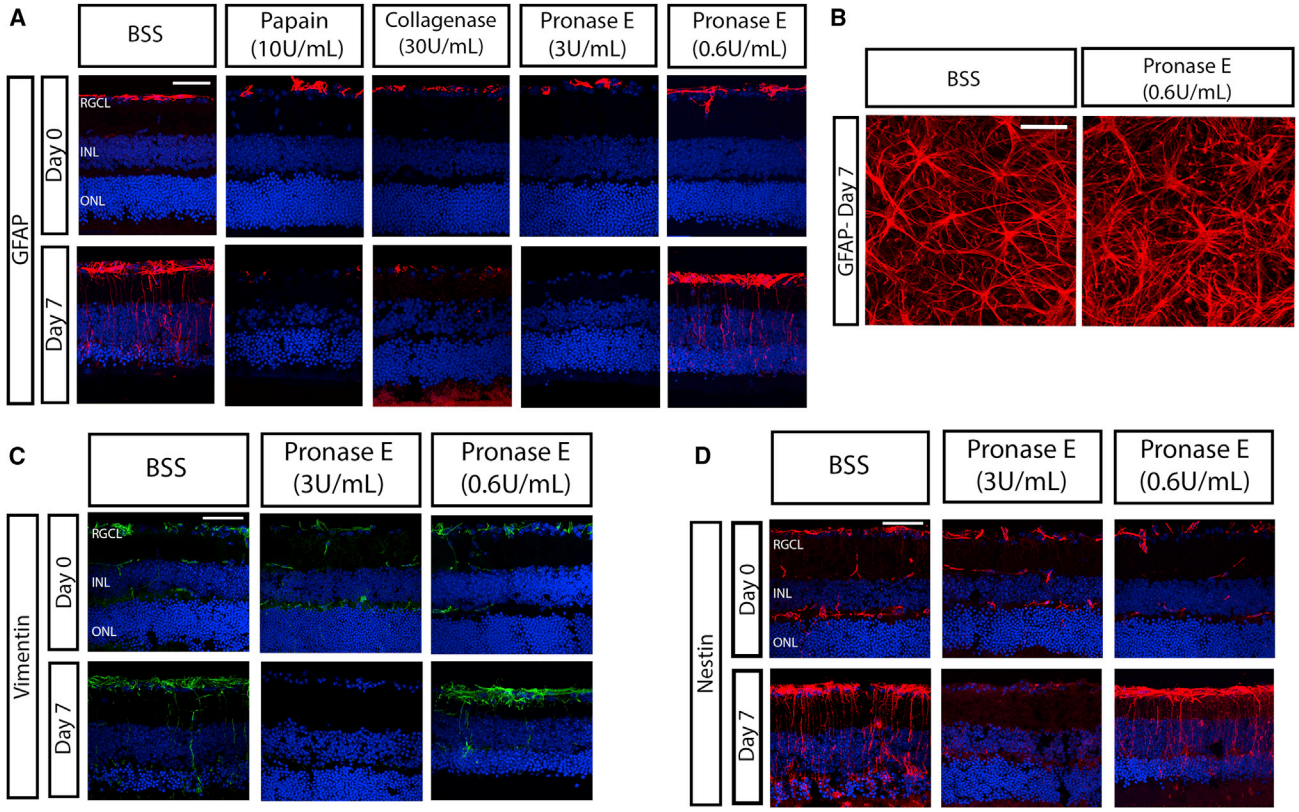

Figure 4. Effect of Proteolytic Enzymes on Glial Reactivity

Adult mouse retinas were explanted and treated with proteolytic enzymes or BSS (negative control) prior to inactivation and washout. Tissue was fixed within 1 h, or after 7 or 11 days of organotypic culture. Glial fibrillary acid protein (GFAP, A, B, red), vimentin (C, green), and nestin (D, red) were upregulated in astrocytes and Müller glia in BSS-treated explants as a result of organotypic culture. Nuclei are counterstained with DAPI (blue). Treatment with papain, collagenase, and pronase E (3 U/mL) resulted in suppression of reactive gliosis, whereas treatment with pronase E (0.6 U/mL) was associated with preservation of reactive gliosis. Scalebars: 50 μm.

areas with focal ILM breaks, without significant changes to the underlying retinal ultrastructure (Figure 3F).

Retinal gliosis impairs intraretinal migration of transplanted MSCs (Johnson et al., 2010). We sought to determine whether proteolytic ILM disruption also affected retinal viability or glial reactivity. Papain caused suppression of retinal gliosis and marked disruption of the laminar retinal architecture by 7–11 days in culture (Figures 3, 4, and S4). Collagenase and pronase E were associated with greater retinal laminar architecture preservation, although glial intermediate filament expression was suppressed after treatment with collagenase or pronase E (3 U/mL) (Figure 4). The lower dose of pronase E (0.6 U/mL), however, caused negligible change to the histological appearance of the retina and was associated with preservation of GFAP, vimentin, and nestin expression in astrocytes and

Figure 3. Effects of Proteolytic Enzymes on the Internal Limiting Membrane

Adult mouse retinas were explanted and treated with proteolytic enzymes or BSS, (negative control) prior to inactivation and washout. Tissue was fixed within 1 h, or after 7 or 11 days of organotypic culture. Laminin (A, B, green), collagen IV (C, red), and alpha-dystroglycan (D, green) were present at the ILM and expression was disrupted to varying degrees by enzyme treatment. Nuclei are counterstained with DAPI (blue). The immunofluorescence of laminin and collagen IV at the ILM were quantified using a qualitative grading scheme or by measuring the percentage linear coverage of the retinal explant surface in cryosections (see Figure S3), which showed ILM disruption by all enzymes tested (E). Transmission electron microscopy of the inner retinal surface reveals intact ILM over Müller glial endfeet in control retinal explants (red arrows), with overlying filaments of posterior vitreous cortex (F). The ILM was absent (top two micrographs) or fragmented (bottom two micrographs) following treatment with pronase E (0.6 U/mL) (blue arrows), without alteration in the structure of the underlying retinal glia. Scalebars: 50 μm (A-D) or as indicated (F). Error bars: SEM (E). *$p < 0.05$, **$p < 0.01$, ***$p < 0.001$ by one-way ANOVA with post-hoc Dunnett's test for multiple comparisons versus the BSS control group.

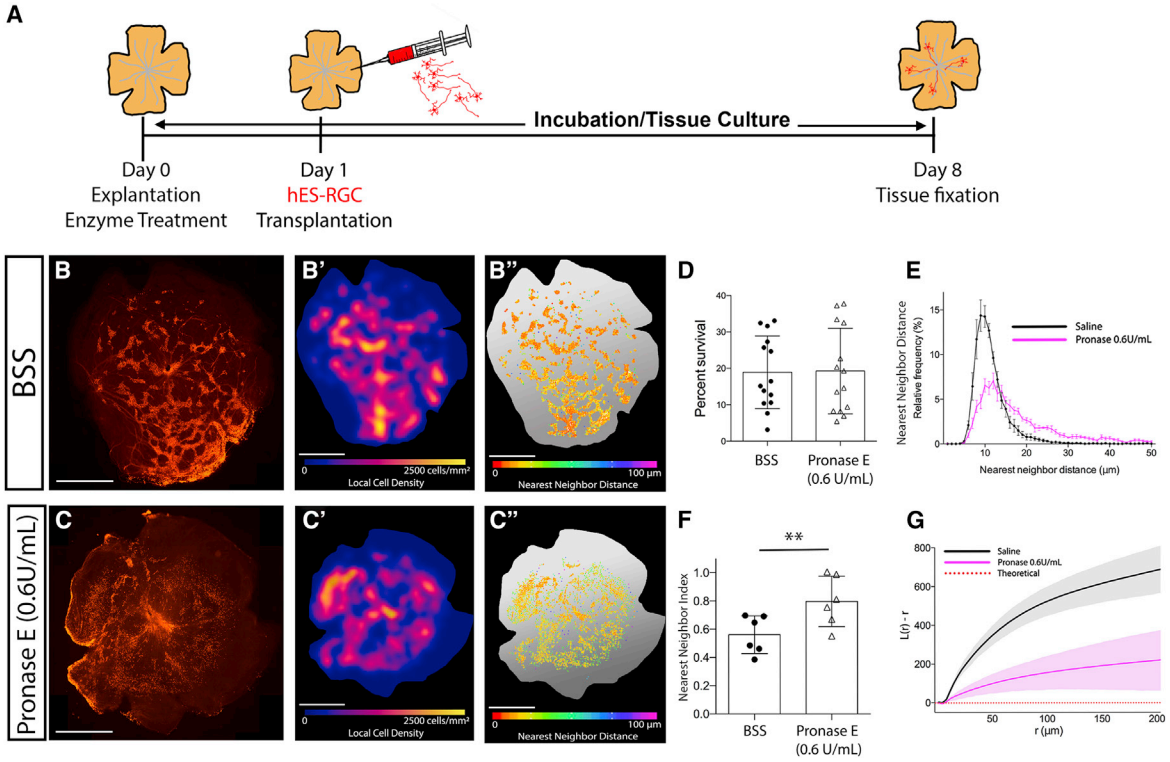

Figure 5. Topographic Spacing of hES-RGCs Co-cultured on Retinal Explants with or without Proteolytic Enzyme Pre-treatment

The experimental paradigm is shown (A). Adult mouse retinas were explanted and treated with proteolytic enzyme or BSS (negative control) prior to inactivation and washout. The following day, hES-RGCs were co-cultured on retinal explants for 1 week prior to analysis. Epifluorescent micrographs show the tdTomato + hES-RGC morphology (B, C). Cell density heatmaps (B′, C′) and NND maps (B″, C″) demonstrate greater cell dispersal with enzyme pre-treatment. hES-RGC survival was similar in both groups (D). NND (E), NN index (F), and Ripley's L function (G) all demonstrated significantly less clustering following proteolytic enzyme treatment. Scalebars: 1.25 mm. Error bars: SD (D, F); SEM (E); 95% confidence interval (G). *$p \leq 0.05$, **$p \leq 0.01$, ***$p \leq 0.001$.

Müller glia (Figure 4). Importantly, since transplanted RGCs would need to synapse with bipolar and amacrine cells, we documented that pronase E (0.6 U/mL) resulted in negligible change to the ultrastructure of the inner plexiform layer (IPL) and INL at day 7 of culture (Figure S5).

In sum, all enzymes tested caused marked and persistent ILM disruption. Papain caused unacceptable neurotoxicity at the concentrations tested. Collagenase and pronase E (3 U/mL) caused less overt structural retinal degradation but suppressed reactive gliosis. Pronase E (0.6 U/mL) effectively digested the ILM without inducing detectable changes to the viability or physiology of the retina.

hES-RGC Survival and Topology Following ILM Disruption

In order to evaluate the effects of proteolytic ECM digestion on co-cultured hES-RGCs, we applied and then inactivated and washed out enzymes ≥24 h prior to addition of hES-RGCs onto the retinal explant surface (Figure 5A). Collagenase and pronase E (3 U/mL) were tested because of their relatively mild effect on retinal explant cytoarchitecture. However, they also negatively affected hES-RGC survival and were associated with high variability in topographic parameters, so further evaluation of these enzymes' effect on survival and topology was not undertaken (Figure S6).

Consistent with its lack of apparent toxicity and in contrast to the other enzyme treatments tested, pronase E (0.6 U/mL) resulted in no change in hES-RGC survival following co-culture compared with BSS (19.2% ± 11.7% vs 18.9% ± 10.0%, respectively, $p = 0.9$, Figure 5D). Pronase E (0.6 U/mL) was associated with dispersed rather than clustered hES-RGC spatial survival patterns (Figures 5B and 5C). Average hES-RGC density on pronase E-treated retinal explants was 210.2 ± 147.1 cell/mm^2 compared with 266.4 ± 196.3 cell/mm^2 for BSS ($p = 0.4$). The average hES-RGC NND of pronase E-treated retinal explants was 24.2 ± 7.2 µm vs 11.7 ± 1.6 µm on control retinal explants (Figure 5E, $p < 0.01$). The NNI was significantly higher in pronase E-treated explants compared with controls, indicating reduced clustering (Figure 5F). L(r)-r demonstrated

a significantly attenuated rise over CSR for hES-RGCs on pronase E-treated retinal explants vs control, indicating reduced spatial clustering with enzymatic ECM disruption (Figure 5G). Nerve fiber bundling from hES-RGCs was not identified in pronase E (0.6 U/mL)-treated explants, unlike in controls (14.9 neurite bundles/100 hES-RGCs, Figures 5B and 5C).

In sum, compared with BSS treatment, pronase E (0.6 U/mL) resulted in greater spatial dispersion of hES-RGCs with no clustering or neurite bundling, and without affecting overall survival, unlike collagenase or pronase E (3 U/mL), which reduced hES-RGC survival.

hES-RGC Neurite Structural Engraftment Following ILM Disruption

ECM digestion resulted in a dramatic increase in hES-RGC neurite localization into the retina after 7 days (Figures 6 and S6). RGC somas, however, generally remained superficial to the retina or localized to the retinal nerve fiber layer (RNFL) or RGCL without migrating deeper. Although collagenase and pronase E (3 U/mL) did increase neurite penetration into the retina, the results were variable and of borderline statistical significance (Figure S6).

Interestingly, pre-treatment with pronase E (0.6 U/mL) led to greater increase in hES-RGC neurite ingrowth into the retina than collagenase or pronase E (3 U/mL), resulting in a more than 40-fold increase in the length and number of neurite segments in the IPL as compared with control explants (Figure 6, Videos S3 and S4). hES-RGC neurites could be found ectopically in the INL and outer nuclear layer (ONL), although to a lesser extent than neurites located in the IPL. In pronase E (0.6 U/mL)-treated retinal explants, there were 3.2-fold more hES-RGC neurites in the IPL than the INL and 6.3-fold more than in the ONL. Total neurite length was 3.2-fold greater in the IPL than the ONL, and 7.3-fold greater than in the ONL. We did not identify transplanted RGCs with dendrites that conformed to the morphology of any traditional RGC subtype.

To assess the possibility that material transfer of tdTomato RNA or protein to endogenous retinal neurons could have led to confusion about the source of the observed tdTomato$^+$ neurites (Nickerson et al., 2018; Pearson et al., 2016; Santos-Ferreira et al., 2016; Singh et al., 2016), we co-cultured hES-RGCs on retinal explants derived from ubiquitously GFP-expressing transgenic mice. We examined 337 hES-RGC somas superficial to the retina and 24 hES-RGC somas that had migrated into the retinal parenchyma, and 40 hES-RGC neurites within the retinal parenchyma using orthogonal confocal projections and fluorescence intensity histograms. We did not identify any presumed hES-RGCs with a neuronal morphology that co-expressed tdTomato and GFP (Figure 7E). Moreover, an antibody that specifically recognizes human nuclei labeled all tdTomato$^+$ hES-RGC somas (Figure 7D), suggesting the tdTomato$^+$ neurites visualized within the recipient retina arose from transplanted hES-RGCs.

Characterization of hES-RGC Neurites within the Neuroretinal Parenchyma

We evaluated subcellular localization of canonical axonal or dendritic proteins in co-cultured hES-RGCs. hES-RGCs universally expressed β-III-tubulin in the cell bodies and processes, regardless of location (Figure 7A). We next evaluated localization of Tau, which is expressed in mature axons, and MAP2, which is expressed in mature dendrites (Figure 7B). Of note, immature developing neurons segregate MAP2 and Tau only after specification of the axon (Dehmelt and Halpain, 2005). Therefore, developing neurons may co-localize these proteins within immature neurites. Within 296 individual neurite processes, we identified a differential expression pattern of MAP2 and Tau that correlated with neurite localization within the host retina. On the retinal surface, Tau and MAP2 were co-expressed in 92.7% of hES-RGC neurites, whereas 6.9% of neurites expressed Tau only. Within the retinal parenchyma, however, 73.5% of neurites co-expressed Tau and MAP2 ($p = 0.001$ vs surface), 20.4% expressed Tau only ($p = 0.005$ vs surface), and 4.1% expressed MAP2 only ($p = 0.069$ vs surface). This observation might suggest that structural localization within the host retina promotes the maturation of hES-RGCs or that localization into the neuroretina follows neurite specification. However, Tau$^+$ axons localizing deep to the RNFL would be ectopic.

To determine the propensity of co-cultured hES-RGC neurites to synapse with recipient retinal neurons, we used immunofluorescence to visualize synaptic proteins colocalizing with hES-RGC neurites. The postsynaptic protein PSD-95 was present in puncta that occasionally colocalized with hES-RGC somas and neurites (Figure 7C). We also identified examples of neurites in the deep retinal layers that expressed PSD-95 in a punctate pattern, consistent with what one would expect from a mature integrated RGC dendrite.

DISCUSSION

While human stem cell-derived RGCs extend neurites following co-culture on explanted retinal tissue, those neurites do not spontaneously localize within the retinal parenchyma. Localization of RGC dendrites to the IPL is a clear necessity for functional synaptogenesis with bipolar and amacrine cells to occur. Our data suggest that the ILM is a key barrier to hES-RGC neurite engraftment in the retina, as mechanical disruption or enzymatic degradation of ILM proteins were associated with marked

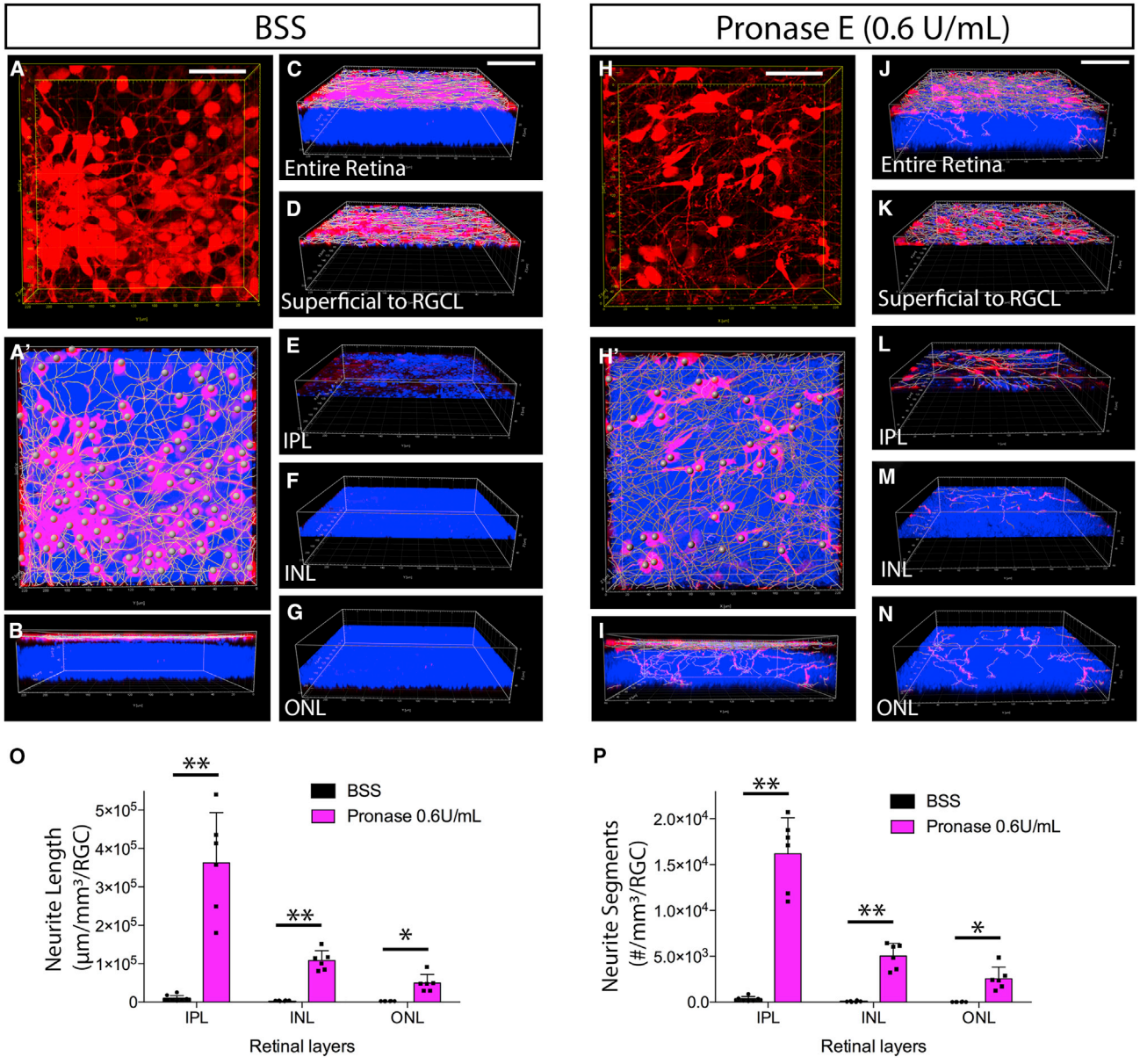

Figure 6. Retinal Neurite Ingrowth from hES-RGCs Co-cultured on Retinal Explants with or without Proteolytic Enzyme Pre-treatment

In saline (BSS, negative control) treated retinal explants, co-cultured hES-RGCs (red) remained superficial to the neural retina, forming a distinct layer on top of the RGCL (A–G). Following pre-treatment with pronase E (0.6 U/mL), hES-RGC neurites extended into the neural retina (H–N). Three-dimensional reconstructions are shown (A–C, H–J) and the reconstructions were segmented according to retinal layer (D–G, K–N) to quantify hES-RGC neurite ingrowth on a spatially localized volumetric basis (O, P). Scalebars: 50 µm. Error bars: SD (O, P). *p $\leq$ 0.05, **p $\leq$ 0.01 by unpaired t test.

increases in retinal neurite ingrowth. Therefore, developing methods to permit donor RGC neurites to bypass the ILM will be critical to the future of RGC replacement. Given the low efficiency of transplanted RGC engraftment documented in the most encouraging work to date (Venugopalan et al., 2016), our data provide a clear avenue toward improving RGC transplantation outcomes in the future using *in vivo* pre-clinical models.

hES-RGC Neurite Engraftment

In untreated retinal explants, we identified virtually no interaction between co-cultured hES-RGCs and underlying

Please cite this article in press as: Zhang et al., Role of the Internal Limiting Membrane in Structural Engraftment and Topographic Spacing of Transplanted Human Stem Cell-Derived Retinal Ganglion Cells, Stem Cell Reports (2020), https://doi.org/10.1016/j.stemcr.2020.12.001

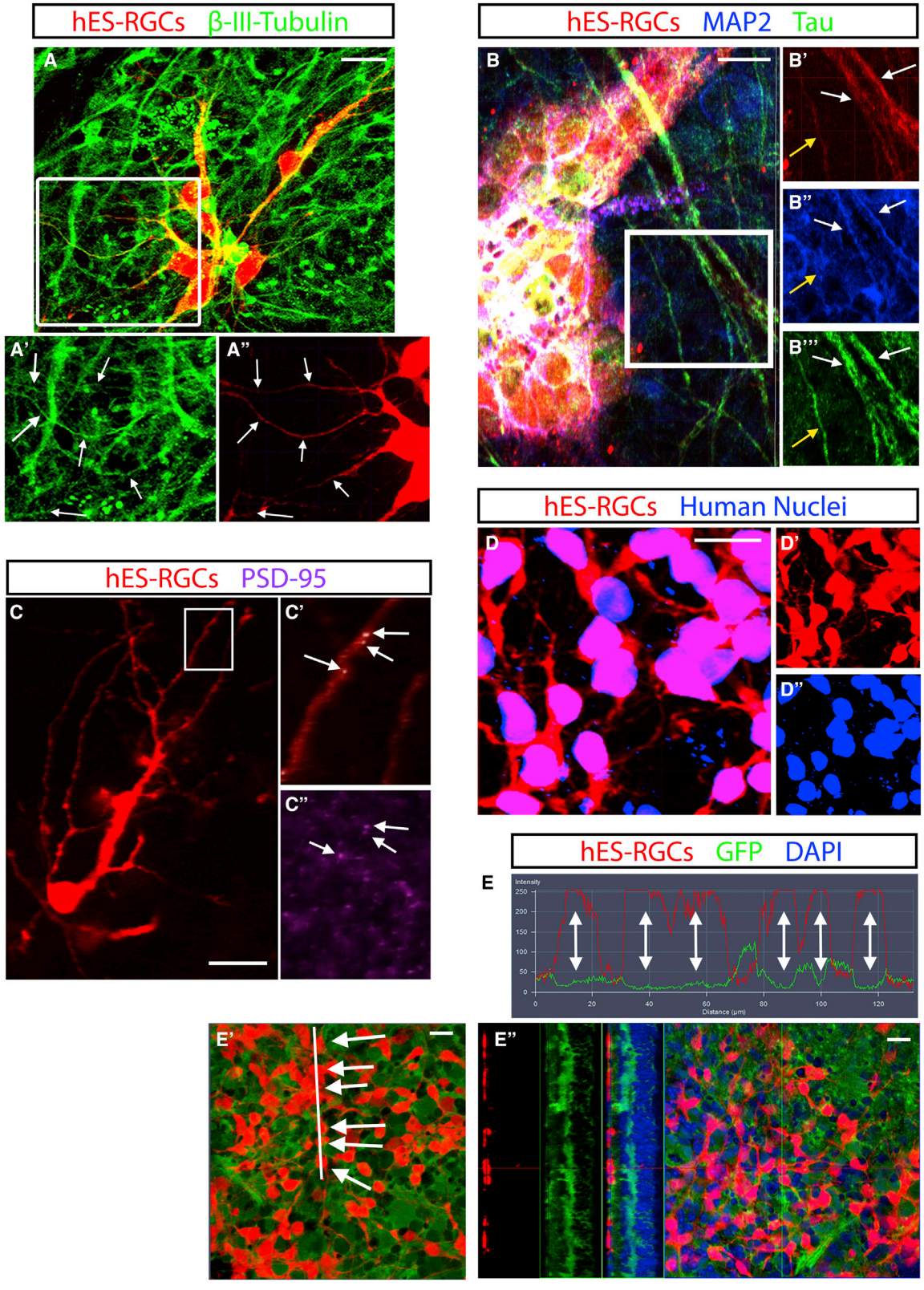

(legend on next page)

retinas, except in locations with physical disruption to the retina and ILM. The mechanical disruption associated with relaxing incisions in retinal explants was significantly more controlled and reproducible than would have been feasible if conducted *in vivo*. In addition, it is noteworthy that the organotypic retinal explant culture model likely biases toward greater engraftment than intravitreal injection *in vivo*, given that transplanted neurons are maintained in direct opposition to the ILM rather than being suspended within the vitreous cavity. Therefore, the exclusion of hES-RGCs from integration under control conditions supports the validity of this system in modeling barriers to intravitreal transplantation.

The ILM limits neuroretinal transduction by intravitreally administered AAV vectors. Experimental enzymatic digestion (Dalkara et al., 2009), surgical ILM peeling (Takahashi et al., 2017; Teo et al., 2018), and sub-ILM injection (Gamlin et al., 2019) circumvent this barrier, although the latter two are likely not feasible in rodent eyes. Here, we demonstrate that enzymatic digestion of ECM proteins within the ILM enhances retinal neurite ingrowth of exogenous RGCs. From a translational perspective, addressing the ILM barrier will be necessary to achieve functional RGC replacement. Given that ILM thickness increases substantially with age and in the presence of common diseases like diabetes (To et al., 2013), patients suffering from age-related optic neuropathies such as glaucoma and ischemic optic neuropathy may have a greater impediment to engraftment. Enzyme administration may not be necessary in pre-clinical large animal models or in human patients, since surgical ILM peeling is a well-established and safe maneuver for the treatment of macular hole (Brooks, 2000). It is also possible that intravitreal proteolytic enzymes would be toxic at the concentrations needed to digest the ILM clinically. For example, we found that intravitreal papain, pronase E, and collagenase at the concentrations used here digested the retinal vasculature and induced intraocular hemorrhage in living mice, although further preliminary data suggest that effective doses of intravitreal pronase E that disrupt the ILM *in vivo* without inducing hemorrhage exist (data not shown). Clearly, additional experiments conducted in living eyes are necessary to substantiate a role of the ILM in transplanted hES-RGC engraftment *in vivo*, and these empiric data provide strong rationale for that work going forward.

We have previously assessed barriers to retinal integration of bone marrow-derived MSCs and noted that, although ILM digestion with collagenase did not permit transplant integration, suppression of reactive gliosis with alpha-aminoadipic acid did (Johnson et al., 2010). In that case, MSCs entered the retina in spite of an intact ILM, suggesting that this structure is not a generalized physical barrier. It is therefore notable that, for hES-RGCs, ILM digestion that specifically preserves glial reactivity dramatically improves structural cell integration. We speculate that differential effects of the ILM and retinal gliosis on engraftment of these two cell types is modulated by differential expression of cell surface receptors that mediate interactions with the ECM and glia. Identification of surface receptors mediating hES-RGC interactions with the ILM could therefore inform methods of permitting trans-ILM retinal integration without the need for disrupting the ILM directly, and this is a subject of ongoing investigation. Indeed, given the importance of RGC-ILM interactions for retinal patterning during development, total disruption of the ILM may in fact be counterproductive. For instance, signaling between developing RGCs and laminin within the ILM is involved in polarity decisions and axon localization to the basal retina, although polarization does persist in the absence of this signaling at a delayed pace (Randlett et al., 2011).

We noted that hES-RGC neurites entering the retinal parenchyma did not exclusively target the IPL. The developmental factors that control RGC dendrite laminar patterning to and within the IPL include both molecular cues and activity-dependent refinement (Tian, 2011). Spontaneous electrophysiological activity in organotypic retinal explants is modest, decreases with time, and may

Figure 7. Characterization of Structurally Integrated hES-RGC Neurites

One week after hES-RGCs (red) were co-cultured on retinal explants, immunofluorescence was used to characterize the transplanted neurons and their neurite processes. Transplanted hES-RGCs universally expressed β-III-tubulin (green) including in their neurites (A, arrows point to neurites co-expressing tdTomato and β-III-tubulin). Of note, β-III-tubulin is also expressed by the surviving endogenous RGCs, which are tdTomato$^-$. Neurites from hES-RGCs almost uniformly expressed Tau (green), but a subset co-expressed MAP2 (blue, (B). White arrows in B indicate Tau$^+$MAP2$^+$ neurites, and the yellow arrow highlights at Tau$^+$MAP2$^-$ neurite. Postsynaptic density-95 (PSD-95, purple, C″) puncta could be found co-localizing with transplanted hES-RGC neurites within the IPL (C). Co-localization confirmed by a thresholding algorithm using Imaris is indicated by white puncta (arrows, C′). hES-RGCs expressing tdTomato were uniformly labeled by antibody recognizing human nuclear antigen (D). hES-RGCs transplanted onto retinal explants isolated from transgenic mice ubiquitously expressing GFP were uniformly GFP negative at the cell soma and within their neurite processes (E), as demonstrated by orthogonal slices (E″) and by immunofluorescence intensity histograms for tdTomato (red) and GFP (green) that demonstrate mutual exclusivity (E). Single-headed arrows (E′) point to cells tested for co-localization in the histogram shown, and double-headed arrows show the immunofluorescence profiles of those cells expressing tdTomato but not GFP (E). Scalebars: 20 μm.

have limited any potential IPL-directed dendrite localization reinforced by neuronal activity (Alarautalahti et al., 2019). During development, RGC dendrites target pre-patterned IPL afferents (Mumm et al., 2006). Sublamination within the IPL is guided by the expression of specific cell surface receptors and their binding to localized lamina-specific ligands, including integrins, cadherins, and plexins, play critical roles in dendritic outgrowth and guidance (Duan et al., 2014; Hocking et al., 2010; Liu et al., 2018; Matsuoka et al., 2011; Peng et al., 2017; Riccomagno et al., 2014; Sun et al., 2013; Yamagata and Sanes, 2008, 2012). It is conceivable that controlling expression of relevant surface receptors may aid in guiding hES-RGC dendrites to specific locations where afferent synaptogenesis may occur. It remains unclear the extent to which ligand expression is maintained within the mature IPL, but the identification of appropriate dendritic stratification by transplanted primary RGCs suggests that at least some of the necessary signals remain present (Venugopalan et al., 2016).

hES-RGC Survival

Consistent with prior reports documenting limited survival and integration of transplanted RGCs (Venugopalan et al., 2016; Wu et al., 2018), we observed hES-RGC survival rates of 10%–30% at one week. Survival was not affected by retinal pre-treatment with pronase E (0.6 U/mL), although it was further reduced by pronase E (3 U/mL) or collagenase, which also impaired retinal glial activity. Our finding that transplanting fewer (1.5×10^4) hES-RGCs was associated with inferior survival compared with transplantation of 2.5×10^4 or 5×10^4 cells is in contrast to the report by Venugopalan et al. (2016) showing that transplanting 4×10^4 RGCs resulted in 3-fold greater survival than 6×10^4 cells. Differences in the source of transplanted RGCs, the recipient species and model system, or the experimental time period following transplantation may explain these findings. Alternatively, the association between transplanted RGC number and survival rate may be represented by an inverted U-shaped curve, where too few or too many transplanted cells are suboptimal. Regardless, improving RGC survival following transplantation is a key goal for ongoing research.

hES-RGC Topographical Localization

We observed a stark difference in spatial clustering of transplanted hES-RGC somas with and without proteolytic enzyme pre-treatment of the recipient retina. Cell clumping on retinal explants, a phenomenon that was not observed in dissociated cell culture, was attenuated by ECM digestion. This might suggest that interactions between hES-RGCs and the ILM promote cell clustering. It is interesting, however, that transgenic disruption of neuronal interactions with the ILM through dystroglycan (Clements et al., 2017), integrin-β1, or Cas adaptor proteins (Riccomagno et al., 2014) results in ectopic clustering of RGCs and amacrine cells on the basal retinal surface. In order to quantify our observation in a statistically robust manner, we employed a number of spatial analytic tools, including NND distributions (which reflect hyperlocal cell relationships between only adjacent cells), DRPs (which provide insight into densities over larger distances), and Ripley functions (cumulative functions that facilitate normalization to CSR conditions and therefore comparisons between experimental groups). While these methods have not been previously applied to retinal neuronal transplantation, the relative strengths and weaknesses of these tools for characterizing endogenous retinal neuron mosaicism have been elegantly reviewed recently (Keeley et al., 2020).

Unlike the clear necessity for hES-RGC dendrites to be proximally localized to bipolar and amacrine processes for synaptogenesis, the significance of hES-RGC soma clustering on intact ILM is unclear. The NND of hES-RGCs within clusters was only marginally lower than that of packed endogenous RGCs, and high-density coverage of the retina may be necessary to obtain high-resolution retinotopic physiology. However, lateral spreading of transplanted hES-RGCs will be necessary to achieve widespread coverage. Whether somal clumping and neurite ingrowth are directly related will need to be determined by future work.

Material Transfer

A critical aspect of this work was the exclusion of material transfer or material exchange as a possible explanation for the presence of tdTomato$^+$ neurites within the host retina. Early photoreceptor transplantation experiments were interpreted as demonstrating a high degree of donor cell integration. However, subsequent experiments demonstrated that labeled donor photoreceptors transplanted into the subretinal space transfer either label RNA or protein to host cells through still-unclear mechanisms, and that most labeled cells in the ONL are actually host derived and secondarily acquire label through material transfer (Nickerson et al., 2018; Pearson et al., 2016; Santos-Ferreira et al., 2016; Singh et al., 2016). Although RGC participation in material transfer has not been reported, it is prudent for all neuronal transplantation work to include control experiments to assess for this phenomenon. In this work, tdTomato$^+$ cells with neuronal morphology transplanted into pan-GFP mice did not express GFP, indicating that they were not host derived. Further, they uniformly expressed human nuclear antigen, consistent with their donor origin.

Limitations

There are several limitations of the organotypic retinal explant system employed in this work, which are critical

to consider in applying these findings to the next steps in RGC transplantation development. While this model has important advantages for initial experimentation, such as higher throughput than living animal models and the ability to precisely control drug concentrations and mechanical ILM disruption, it is ultimately a stepping-stone in clinical translation to more complex model systems. Retinal explants possess a temporal limit to the viability of the host tissue of about 10–14 days in culture, which restricts experimental duration to less than might be required for functional synaptogenesis. Moreover, spontaneous and light-responsive electrophysiologic activity of the endogenous retinal neurons are lost over time in retinal explants (Alarautalahti et al., 2019)which precludes our ability to demonstrate true functional integration of hES-RGCs in this system. Although the inability of RGC neurites to localize to the retinal parenchyma in the presence of an intact ILM clearly prohibits their function within the visual pathway, permissive neurite ingrowth documented here following ILM disruption does not necessarily imply that functional wiring into the host retina will occur. This must be assessed further in living animal models. Additional obstacles may be present in the living eye that could not be modeled *ex vivo*. The expression of important chemotactic or inhibitory factors may change in retinal explants as compared with *in vivo* retina, as this has not been specifically evaluated. There is no circulation or immune system in retinal explants, so immunologic rejection could not be modeled here. As such, future work conducted *in vivo* will need to overcome additional obstacles to the integration of transplanted RGCs into the retinal neurocircuitry. However, the identification of the ILM as a primary barrier will be critical to those future experiments and the data provided here suggest a pragmatic approach to increase the efficiency of transplanted RGC engraftment. Also of note, this work does not address axon outgrowth, pathfinding, or efferent synaptogenesis. Such studies await efficient engraftment of transplanted RGCs in an *in vivo* model.

Conclusions

We have characterized the spontaneous morphologic behavior of exogenous hES-RGCs introduced onto mammalian neurosensory retina. Co-cultured cells demonstrate clustering of cell somas, bundling of nerve fibers, and exclusion of neurites from the retinal parenchyma. Proteolytic digestion of ECM proteins within the ILM is associated with reduced cell body clustering, a lack of fiber bundling, and a profound increase in neurite ingrowth into the retina. It is likely that modifying the interactions between transplanted RGCs and the ILM will be necessary to facilitate efficient functional engraftment for RGC replacement and optic nerve regeneration.

EXPERIMENTAL PROCEDURES

Animals

Adult (age 8–16 weeks) CD1 mice or C57BL/6-Tg(CAG-EGFP)10sb/J mice that express GFP ubiquitously (Jackson Laboratories, Bar Harbor, ME) of both sexes were used. Animals were housed in environmentally controlled (12-h light/dark cycle) conditions with food and water available *ad libitum*. All experimental procedures were approved by Johns Hopkins University's Animal Care and Use Committee.

Human Stem Cell-Derived RGCs

Human H9 ES cells (WiCell, Madison, WI) carrying genes for tdTomato and the murine cell-surface protein CD90.2/THY1.2 driven by the endogenous *POU4F2* (*BRN3B*) promoter were clonally propagated in mTeSR-1 media (StemCell Technologies, Cambridge, MA) on growth factor-reduced Matrigel substrate (Corning, Corning, NY), in 10% CO_2/5% O_2. Differentiation to RGC fate and immunopurification were performed as described previously (Sluch et al., 2017). This work was approved by Johns Hopkins University's Institutional Stem Cell Research Oversight Committee. See Supplemental Experimental Procedures.

Organotypic Retinal Explants

Neural retina was separated from the retinal pigmented epithelium and flat mounted for culture on polytetrafluoroethylene organotypic filters (Millipore-Sigma, Burlington, MA) with the photoreceptor side against the membrane, as described previously (Bull et al., 2011; Johnson et al., 2010, 2016; Johnson and Martin, 2008). See Supplemental Experimental Procedures.

Proteolytic Enzymes

Proteolytic enzymes in 5-μL aliquots were applied to the inner (vitreous) surface of organotypic retinal explants and incubated for 30–60 min at 37°C, inactivated by bathing explants in ovomucoid (10 mg/mL, Millipore-Sigma) and BSA (10 mg/mL, Millipore-Sigma) in BSS for 5 min at 37°C, washed twice in PBS, and placed back into culture media. RGC transplantation occurred $\geq$24 h later. See Supplemental Experimental Procedures.

Light Microscopy

All samples were reassigned random identification numbers by a second investigator to mask the microscopist and ensure unbiased field selection for imaging. Unmasking occurred only after microscopy and image analysis. Cryosections and retinal explant flat mounts were imaged using confocal laser scanning microscopes (Models 510 or 710, Carl Zeiss Microscopy, Thornwood, NY). Images were obtained with a Plan-Apochromat 40×/1.3 Oil DIC M27 objective, measured 212.34 μm × 212.34 μm (x, y), and were acquired with voxel size 0.208 μm × 0.208 μm × 0.449 μm (x, y, z). The pinhole was set to 1 Airy unit. Random fields of retinal explant flat mounts were selected for microscopy, but areas of retina within 300 μm of the tissue edge, relaxing incisions, or any obvious tissue trauma were excluded when assessing the effects of proteolytic enzymes.

Cryosections and flat mounts underwent epifluorescent imaging using an EVOS microscope (Life Technologies, Grand Island, NY).

Individual fields were manually focused and imaged using the 20× objective. Image tiles were stitched to form one single image per sample. Retinal explant cryosections and retinal flat mounts were imaged and analyzed in their entirety (i.e., not sampled).

Image Analyses

Topographic localization of RGCs on retinal explants was analyzed using ImageJ (v1.52u, NIH, Bethesda, MD). NN distance was determined using a script developed for ImageJ (Mao, 2016). DRPs were generated using the sjedrp R package (Stephen Eglen, University of Cambridge) (Rodieck, 1991). L(r)-r derivatives of Ripley's *K* function were generated using the Lest function from the R spatstat package.

Analyses of hES-RGC neurites were performed using Imaris (v9.3, Oxford Instruments, Zurich, Switzerland). To parse neurite localization according to retinal layer, 3D reconstructions were visualized and rectangular surfaces were created manually spanning the x-y dimensions of the image volume, with z dimensions corresponding to retinal layer boundaries visualized by DAPI stain, which included a superficial layer that included cells external to the retina and within the RNFL and RGCL, IPL, INL, and ONL. Resolving the outer plexiform layer or the RGCL separately from the overlying superficial layer of transplanted cells was attempted and inconsistent across entire 3D reconstructed volumes due to tissue undulation. hES-RGC neurites superficial to the retina, within the RNFL, or within the RGCL would all be incapable of synapsing within afferent retinal neurons in the IPL and therefore were treated similarly. The tdTomato signal was masked according to retinal layer surface. Neurites were traced in a semi-manual manner using the filament workflow and the autopath tool.

hES-RGC soma localization within recipient retina was assessed in Zen software (v8.1.0, 2012 SP1, Carl Zeiss Microscopy) using z stack scrolling and orthogonal projections. Co-localization between tdTomato and GFP was evaluated in Zen using co-localization histograms and orthogonal projection. Co-localization between tdTomato and PSD-95 puncta was evaluated in Imaris using the co-localization tool.

Statistical Analyses

Data are reported as mean ± SD unless otherwise stated. At least 4–6 independent organotypic retinal explant cultures were analyzed per group. Each experiment was performed at least twice. Group means were compared using unpaired two-tailed t tests or one-way ANOVA, and pairwise comparisons were made with Dunnett's post hoc tests with corrections for multiple comparisons with a single control group. Chi-square tests were used to compare the frequencies of gene expression within hES-RGCs according to retinal localization. Following correction for multiple comparisons, $p < 0.05$ was considered statistically significant. Data were analyzed using SPSS (v25, IBM Corp, Armonk, NY) and plotted using Prism (v8.0, GraphPad Software, San Diego, CA). The data that support the findings of this study are available from the corresponding author upon reasonable request.

SUPPLEMENTAL INFORMATION

Supplemental Information can be found online at https://doi.org/10.1016/j.stemcr.2020.12.001.

AUTHOR CONTRIBUTIONS

Collection/assembly of data, data analysis and interpretation, manuscript writing, final manuscript approval, K.Y.Z. Collection/assembly of data, data analysis and interpretation, manuscript writing, and final manuscript approval, C.T. Provision of study material, manuscript writing, final approval of manuscript, J.L.M. Collection and assembly of data, manuscript writing, final approval of manuscript, S.Q. Data analysis and interpretation, final approval of manuscript, L.W. Financial support, provision of study material, data analysis and interpretation, final approval of manuscript, H.A.Q. Financial support, provision of study material, data analysis and interpretation, final approval of manuscript, D.L.Z. Conception and design, financial support, administrative support, provision of study material, collection and assembly of data, data analysis and interpretation, manuscript writing, final approval of manuscript, T.V.J.

DECLARATION OF INTERESTS

The authors declare no competing interests.

ACKNOWLEDGMENTS

This work was funded by the National Eye Institute (K12EY015025 [T.J.]; K08EY031801 [T.J.]; R01EY002120 [H.Q.]; P30EY001765 [D.Z.]); The ARVO David L Epstein Award (H.Q. and T.J.); Research to Prevent Blindness (Career Development Award [T.J.] and Unrestricted Grant Funding [Wilmer Eye Institute]); The American Glaucoma Society (Mentoring for the Advancement of Physician Scientists Grant [T.J.]); The Johns Hopkins Physician Scientist Training Program (Pilot Grant [T.J.]); and generous gifts from the Guerrieri Family Foundation, the Gilbert Family Foundation, and the Marion & Robert Rosenthal Family Foundation. The authors are grateful to Dr. Alex Kolodkin (Department of Neuroscience, Johns Hopkins University) for critical evaluation of the manuscript.

Received: August 24, 2020
Revised: November 30, 2020
Accepted: December 1, 2020
Published: December 30, 2020

REFERENCES

Alarautalahti, V., Ragauskas, S., Hakkarainen, J.J., Uusitalo-Jorvinen, H., Uusitalo, H., Hyttinen, J., Kalesnykas, G., and Nymark, S. (2019). Viability of mouse retinal explant cultures assessed by preservation of functionality and morphology. Invest. Ophthalmol. Vis. Sci. *60*, 1914–1927.

Barber, A.C., Hippert, C., Duran, Y., West, E.L., Bainbridge, J.W., Warre-Cornish, K., Luhmann, U.F., Lakowski, J., Sowden, J.C., Ali, R.R., et al. (2013). Repair of the degenerate retina by photoreceptor transplantation. Proc. Natl. Acad. Sci. U S A *110*, 354–359.

Barnea-Cramer, A.O., Wang, W., Lu, S.J., Singh, M.S., Luo, C., Huo, H., McClements, M.E., Barnard, A.R., MacLaren, R.E., and Lanza, R. (2016). Function of human pluripotent stem cell-derived photoreceptor progenitors in blind mice. Sci. Rep. *6*, 29784.

Becker, S., Eastlake, K., Jayaram, H., Jones, M.F., Brown, R.A., McLellan, G.J., Charteris, D.G., Khaw, P.T., and Limb, G.A. (2016). Allogeneic transplantation of muller-derived retinal ganglion cells improves retinal function in a feline model of ganglion cell depletion. Stem Cell Transl. Med. *5*, 192–205.

Beros, J., Rodger, J., and Harvey, A.R. (2018). Developmental retinal ganglion cell death and retinotopicity of the murine retinocollicular projection. Dev. Neurobiol. *78*, 51–60.

Boye, S.E., Alexander, J.J., Witherspoon, C.D., Boye, S.L., Peterson, J.J., Clark, M.E., Sandefer, K.J., Girkin, C.A., Hauswirth, W.W., and Gamlin, P.D. (2016). Highly efficient delivery of adeno-associated viral vectors to the primate retina. Hum. Gene Ther. *27*, 580–597.

Brooks, H.L. (2000). Macular hole surgery with and without internal limiting membrane peeling. Ophthalmology *107*, 1939–1948.

Bull, N.D., Johnson, T.V., Welsapar, G., DeKorver, N.W., Tomarev, S.I., and Martin, K.R. (2011). Use of an adult rat retinal explant model for screening of potential retinal ganglion cell neuroprotective therapies. Invest. Ophthalmol. Vis. Sci. *52*, 3309–3320.

Chao, J.R., Lamba, D.A., Klesert, T.R., La Torre, A., Hoshino, A., Taylor, R.J., Jayabalu, A., Engel, A.L., Khuu, T.H., Wang, R.K., et al. (2017). Transplantation of human embryonic stem cell- derived retinal cells into the subretinal space of a non- human primate. Transl. Vis. Sci. Techn. *6*, 4.

Cho, J.H., Mao, C.A., and Klein, W.H. (2012). Adult mice transplanted with embryonic retinal progenitor cells: new approach for repairing damaged optic nerves. Mol. Vis. *18*, 2658–2672.

Clark, P.J., and Evans, F.C. (1954). Distance to nearest neighbor as a measure of spatial relationships in populations. Ecology *35*, 445–453.

Clements, R., Turk, R., Campbell, K.P., and Wright, K.M. (2017). Dystroglycan maintains inner limiting membrane integrity to coordinate retinal development. J. Neurosci. *37*, 8559–8574.

Dalkara, D., Kolstad, K.D., Caporale, N., Visel, M., Klimczak, R.R., Schaffer, D.V., and Flannery, J.G. (2009). Inner limiting membrane barriers to AAV-mediated retinal transduction from the vitreous. Mol. Ther. *17*, 2096–2102.

Daniszewski, M., Senabouth, A., Nguyen, Q.H., Crombie, D.E., Lukowski, S.W., Kulkarni, T., Sluch, V.M., Jabbari, J.S., Chamling, X., Zack, D.J., et al. (2018). Single cell RNA sequencing of stem cell-derived retinal ganglion cells. Sci. Data *5*, 180013.

Davis, B.M., Guo, L., Brenton, J., Langley, L., Normando, E.M., and Cordeiro, M.F. (2016). Automatic quantitative analysis of experimental primary and secondary retinal neurodegeneration: implications for optic neuropathies. Cell Death Discov. *2*, 16031.

Dehmelt, L., and Halpain, S. (2005). The MAP2/Tau family of microtubule-associated proteins. Genome Biol. *6*, 204.

Divya, M.S., Rasheed, V.A., Schmidt, T., Lalitha, S., Hattar, S., and James, J. (2017). Intraocular injection of ES cell-derived neural progenitors improve visual function in retinal ganglion cell-depleted mouse models. Front. Cell. Neurosci. *11*, 295.

Duan, X., Krishnaswamy, A., De la Huerta, I., and Sanes, J.R. (2014). Type II cadherins guide assembly of a direction-selective retinal circuit. Cell *158*, 793–807.

Edwards, M.M., Mammadova-Bach, E., Alpy, F., Klein, A., Hicks, W.L., Roux, M., Simon-Assmann, P., Smith, R.S., Orend, G., Wu, J., et al. (2010). Mutations in Lama1 disrupt retinal vascular development and inner limiting membrane formation. J. Biol. Chem. *285*, 7697–7711.

Edwards, M.M., McLeod, D.S., Grebe, R., Heng, C., Lefebvre, O., and Lutty, G.A. (2011). Lama1 mutations lead to vitreoretinal blood vessel formation, persistence of fetal vasculature, and epiretinal membrane formation in mice. BMC Dev. Biol. *11*, 60.

Gagliardi, G., Ben M'Barek, K., Chaffiol, A., Slembrouck-Brec, A., Conart, J.B., Nanteau, C., Rabesandratana, O., Sahel, J.A., Duebel, J., Orieux, G., et al. (2018). Characterization and transplantation of CD73-positive photoreceptors isolated from human iPSC-derived retinal organoids. Stem Cell Rep. *11*, 665–680.

Gamlin, P.D., Alexander, J.J., Boye, S.L., Witherspoon, C.D., and Boye, S.E. (2019). SubILM injection of AAV for gene delivery to the retina. Methods Mol. Biol. *1950*, 249–262.

Gonzalez-Cordero, A., Kruczek, K., Naeem, A., Fernando, M., Kloc, M., Ribeiro, J., Goh, D., Duran, Y., Blackford, S.J.I., Abelleira-Hervas, L., et al. (2017). Recapitulation of human retinal development from human pluripotent stem cells generates transplantable populations of cone photoreceptors. Stem Cell Rep. *9*, 820–837.

Halfter, W., Sebag, J., and Cunningham, E.T. (2014). II.E. Vitreoretinal interface and inner limiting membrane. In Vitreous: In Health and Disease, J. Sebag, ed. (Springer New York), pp. 165–191.

Hertz, J., Qu, B., Hu, Y., Patel, R.D., Valenzuela, D.A., and Goldberg, J.L. (2014). Survival and integration of developing and progenitor-derived retinal ganglion cells following transplantation. Cell Transpl. *23*, 855–872.

Hocking, J.C., Hehr, C.L., Bertolesi, G.E., Wu, J.Y., and McFarlane, S. (2010). Distinct roles for Robo2 in the regulation of axon and dendrite growth by retinal ganglion cells. Mech. Dev. *127*, 36–48.

Icha, J., Kunath, C., Rocha-Martins, M., and Norden, C. (2016). Independent modes of ganglion cell translocation ensure correct lamination of the zebrafish retina. J. Cell Biol. *215*, 259–275.

Johnson, T.V., Bull, N.D., and Martin, K.R. (2010). Identification of barriers to retinal engraftment of transplanted stem cells. Invest. Ophthalmol. Vis. Sci. *51*, 960–970.

Johnson, T.V., and Martin, K.R. (2008). Development and characterization of an adult retinal explant organotypic tissue culture system as an in vitro intraocular stem cell transplantation model. Invest. Ophthalmol. Vis. Sci. *49*, 3503–3512.

Johnson, T.V., Oglesby, E.N., Steinhart, M.R., Cone-Kimball, E., Jefferys, J., and Quigley, H.A. (2016). Time-lapse retinal ganglion cell dendritic field degeneration imaged in organotypic retinal explant culture. Invest. Ophthalmol. Vis. Sci. *57*, 253–264.

Jones, I., Hagglund, A.C., and Carlsson, L. (2019). Reduced mTORC1-signalling in retinal progenitor cells leads to visual pathway dysfunction. Biol. Open *8*, bio044370.

Keeley, P.W., Eglen, S.J., and Reese, B.E. (2020). From random to regular: variation in the patterning of retinal mosaics. J. Comp. Neurol. *466*, 343–355.

Kurimoto, Y., Shibuki, H., Kaneko, Y., Ichikawa, M., Kurokawa, T., Takahashi, M., and Yoshimura, N. (2001). Transplantation of adult rat hippocampus-derived neural stem cells into retina injured by transient ischemia. Neurosci. Lett. *306*, 57–60.

Lee, J., Choi, S.H., Kim, Y.B., Jun, I., Sung, J.J., Lee, D.R., Kim, Y.I., Cho, M.S., Byeon, S.H., Kim, D.S., et al. (2018). Defined conditions for differentiation of functional retinal ganglion cells from human pluripotent stem cells. Invest. Ophthalmol. Vis. Sci. *59*, 3531–3542.

Li, Y.Q., Andereggen, L., Yuki, K., Omura, K., Yin, Y.Q., Gilbert, H.Y., Erdogan, B., Asdourian, M.S., Shrock, C., De Lima, S., et al. (2017). Mobile zinc increases rapidly in the retina after optic nerve injury and regulates ganglion cell survival and optic nerve regeneration. Proc. Natl. Acad. Sci. U S A *114*, E209–E218.

Lim, J.H.A., Stafford, B.K., Nguyen, P.L., Lien, B.V., Wang, C., Zukor, K., He, Z.G., and Huberman, A.D. (2016). Neural activity promotes long-distance, target-specific regeneration of adult retinal axons. Nat. Neurosci. *19*, 1073.

Lin, B., McLelland, B.T., Mathur, A., Aramant, R.B., and Seiler, M.J. (2018). Sheets of human retinal progenitor transplants improve vision in rats with severe retinal degeneration. Exp. Eye Res. *174*, 13–28.

Liu, J.Y., Reggiani, J.D.S., Laboulaye, M.A., Pandey, S., Chen, B., Rubenstein, J.L.R., Krishnaswamy, A., and Sanes, J.R. (2018). Tbr1 instructs laminar patterning of retinal ganglion cell dendrites. Nat. Neurosci. *21*, 659.

MacLaren, R.E., Pearson, R.A., MacNeil, A., Douglas, R.H., Salt, T.E., Akimoto, M., Swaroop, A., Sowden, J.C., and Ali, R.R. (2006). Retinal repair by transplantation of photoreceptor precursors. Nature *444*, 203–207.

Mao, Y. (2016). Nearest Neighbor Distances Calculation with ImageJ. https://icme.hpc.msstate.edu/mediawiki/index.php/Nearest_Neighbor_Distances_Calculation_with_ImageJ.html.

Matsuoka, R.L., Nguyen-Ba-Charvet, K.T., Parray, A., Badea, T.C., Chedotal, A., and Kolodkin, A.L. (2011). Transmembrane semaphorin signalling controls laminar stratification in the mammalian retina. Nature *470*, 259–263.

McCabe, K.L., Gunther, E.C., and Reh, T.A. (1999). The development of the pattern of retinal ganglion cells in the chick retina: mechanisms that control differentiation. Development *126*, 5713–5724.

Miltner, A.M., and La Torre, A. (2019). Retinal ganglion cell replacement: current status and challenges ahead. Dev. Dyn. *248*, 118–128.

Moore, D.L., Blackmore, M.G., Hu, Y., Kaestner, K.H., Bixby, J.L., Lemmon, V.P., and Goldberg, J.L. (2009). KLF family members regulate intrinsic axon regeneration ability. Science *326*, 298–301.

Mumm, J.S., Williams, P.R., Godinho, L., Koerber, A., Pittman, A.J., Roeser, T., Chien, C.B., Baier, H., and Wong, R.O.L. (2006). In vivo imaging reveals dendritic targeting of laminated afferents by zebrafish retinal ganglion cells. Neuron *52*, 609–621.

Nickerson, P.E.B., Ortin-Martinez, A., and Wallace, V.A. (2018). Material exchange in photoreceptor transplantation: updating our understanding of donor/host communication and the future of cell engraftment science. Front. Neural Circuit *12*, 17.

Nishida, A., Takahashi, M., Tanihara, H., Nakano, I., Takahashi, J.B., Mizoguchi, A., Ide, C., and Honda, Y. (2000). Incorporation and differentiation of hippocampus-derived neural stem cells transplanted in injured adult rat retina. Invest. Ophthalmol. Vis. Sci. *41*, 4268–4274.

Park, K.K., Liu, K., Hu, Y., Smith, P.D., Wang, C., Cai, B., Xu, B.G., Connolly, L., Kramvis, I., Sahin, M., et al. (2008). Promoting axon regeneration in the adult CNS by modulation of the PTEN/mTOR pathway. Science *322*, 963–966.

Pearson, R.A., Barber, A.C., Rizzi, M., Hippert, C., Xue, T., West, E.L., Duran, Y., Smith, A.J., Chuang, J.Z., Azam, S.A., et al. (2012). Restoration of vision after transplantation of photoreceptors. Nature *485*, 99–103.

Pearson, R.A., Gonzalez-Cordero, A., West, E.L., Ribeiro, J.R., Aghaizu, N., Goh, D., Sampson, R.D., Georgiadis, A., Waldron, P.V., Duran, Y., et al. (2016). Donor and host photoreceptors engage in material transfer following transplantation of post-mitotic photoreceptor precursors. Nat. Commun. *7*, 13029.

Peng, Y.R., Shekhar, K., Yan, W.J., Herrmann, D., Sappington, A., Bryman, G.S., van Zyl, T., Do, M.T.H., Regev, A., and Sanes, J.R. (2019). Molecular classification and comparative taxonomics of foveal and peripheral cells in primate retina. Cell *176*, 1222.

Peng, Y.R., Tran, N.M., Krishnaswamy, A., Kostadinov, D., Martersteck, E.M., and Sanes, J.R. (2017). Satb1 regulates contactin 5 to pattern dendrites of a mammalian retinal ganglion cell. Neuron *95*, 869–883 e866.

Peynshaert, K., Devoldere, J., Minnaert, A.K., De Smedt, S.C., and Remaut, K. (2019). Morphology and composition of the inner limiting membrane: species-specific variations and relevance toward drug delivery research. Curr. Eye Res. *44*, 465–475.

Quigley, H.A., and Broman, A.T. (2006). The number of people with glaucoma worldwide in 2010 and 2020. Br. J Ophthalmol. *90*, 262–267.

Randlett, O., Poggi, L., Zolessi, F.R., and Harris, W.A. (2011). The oriented emergence of axons from retinal ganglion cells is directed by laminin contact in vivo. Neuron *70*, 266–280.

Riccomagno, M.M., Sun, L.O., Brady, C.M., Alexandropoulos, K., Seo, S., Kurokawa, M., and Kolodkin, A.L. (2014). Cas adaptor proteins organize the retinal ganglion cell layer downstream of integrin signaling. Neuron *81*, 779–786.

Rodieck, R.W. (1991). The density recovery profile - a method for the analysis of points in the plane applicable to retinal studies. Vis. Neurosci. *6*, 95–111.

Santos-Ferreira, T., Llonch, S., Borsch, O., Postel, K., Haas, J., and Ader, M. (2016). Retinal transplantation of photoreceptors results in donor-host cytoplasmic exchange. Nat. Commun. *7*, 13028.

Singh, M.S., Balmer, J., Barnard, A.R., Aslam, S.A., Moralli, D., Green, C.M., Barnea-Cramer, A., Duncan, I., and MacLaren, R.E. (2016). Transplanted photoreceptor precursors transfer proteins to host photoreceptors by a mechanism of cytoplasmic fusion. Nat. Commun. *7*, 13537.

Singh, M.S., Issa, P.C., Butler, R., Martin, C., Lipinski, D.M., Sekaran, S., Barnard, A.R., and MacLaren, R.E. (2013). Reversal of end-stage retinal degeneration and restoration of visual function by photoreceptor transplantation. Proc. Natl. Acad. Sci. U S A *110*, 1101–1106.

Singhal, S., Bhatia, B., Jayaram, H., Becker, S., Jones, M.F., Cottrill, P.B., Khaw, P.T., Salt, T.E., and Limb, G.A. (2012). Human muller

glia with stem cell characteristics differentiate into retinal ganglion cell (RGC) precursors in vitro and partially restore RGC function in vivo following transplantation. Stem Cell Transl. Med. *1*, 188–199.

Singhal, S., Lawrence, J.M., Bhatia, B., Ellis, J.S., Kwan, A.S., MacNeil, A., Luthert, P.J., Fawcett, J.W., Perez, M.T., Khaw, P.T., et al. (2008). Chondroitin sulfate proteoglycans and microglia prevent migration and integration of grafted Muller stem cells into degenerating retina. Stem Cells *26*, 1074–1082.

Sluch, V.M., Chamling, X., Liu, M.M., Berlinicke, C.A., Cheng, J., Mitchell, K.L., Welsbie, D.S., and Zack, D.J. (2017). Enhanced stem cell differentiation and immunopurification of genome engineered human retinal ganglion cells. Stem Cell Transl. Med. *6*, 1972–1986.

Sluch, V.M., Davis, C.H.O., Ranganathan, V., Kerr, J.M., Krick, K., Martin, R., Berlinicke, C.A., Marsh-Armstrong, N., Diamond, J.S., Mao, H.Q., et al. (2015). Differentiation of human ESCs to retinal ganglion cells using a CRISPR engineered reporter cell line. Sci. Rep. *5*, 16595.

Sun, L.O., Jiang, Z., Rivlin-Etzion, M., Hand, R., Brady, C.M., Matsuoka, R.L., Yau, K.W., Feller, M.B., and Kolodkin, A.L. (2013). On and off retinal circuit assembly by divergent molecular mechanisms. Science *342*, 1241974.

Takahashi, K., Igarashi, T., Miyake, K., Kobayashi, M., Yaguchi, C., Iijima, O., Yamazaki, Y., Katakai, Y., Miyake, N., Kameya, S., et al. (2017). Improved intravitreal AAV-mediated inner retinal gene transduction after surgical internal limiting membrane peeling in cynomolgus monkeys. Mol. Ther. *25*, 296–302.

Teo, K.Y.C., Lee, S.Y., Barathi, A.V., Tun, S.B.B., Tan, L., and Constable, I.J. (2018). Surgical removal of internal limiting membrane and layering of AAV vector on the retina under air enhances gene transfection in a nonhuman primate. Invest. Ophthalmol. Vis. Sci. *59*, 3574–3583.

Teotia, P., Chopra, D.A., Dravid, S.M., Van Hook, M.J., Qiu, F., Morrison, J., Rizzino, A., and Ahmad, I. (2017). Generation of functional human retinal ganglion cells with target specificity from pluripotent stem cells by chemically defined recapitulation of developmental mechanism. Stem Cells *35*, 572–585.

Tham, Y.C., Li, X., Wong, T.Y., Quigley, H.A., Aung, T., and Cheng, C.Y. (2014). Global prevalence of glaucoma and projections of glaucoma burden through 2040 A systematic review and meta-analysis. Ophthalmology *121*, 2081–2090.

Tian, N. (2011). Developmental mechanisms that regulate retinal ganglion cell dendritic morphology. Dev. Neurobiol. *71*, 1297–1309.

To, M., Goz, A., Camenzind, L., Oertle, P., Candiello, J., Sullivan, M., Henrich, P.B., Loparic, M., Safi, F., Eller, A., et al. (2013). Diabetes-induced morphological, biomechanical, and compositional changes in ocular basement membranes. Exp. Eye Res. *116*, 298–307.

Upton, A.L., Cordery, P.M., and Thompson, I.D. (2007). Emergence of topography in the developing hamster retinocollicular projection: axial differences and the role of cell death. Eur. J. Neurosci. *25*, 2319–2328.

Venugopalan, P., Wang, Y., Nguyen, T., Huang, A., Muller, K.J., and Goldberg, J.L. (2016). Transplanted neurons integrate into adult retinas and respond to light. Nat. Commun. *7*, 10472.

Wang, S.T., Chen, L.L., Zhang, P., Wang, X.B., Sun, Y., Ma, L.X., Liu, Q., and Zhou, G.M. (2019a). Transplantation of retinal progenitor cells from optic cup-like structures differentiated from human embryonic stem cells in vitro and in vivo generation of retinal ganglion-like cells. Stem Cells Dev. *28*, 258–267.

Wang, X.W., Yang, S.G., Zhang, C., Hu, M.W., Qian, J., Ma, J.J., Zhang, Y., Yang, B.B., Weng, Y.L., Ming, G.L., et al. (2020). Knocking out non-muscle myosin II in retinal ganglion cells promotes long-distance optic nerve regeneration. Cell Rep. *31*, 107537.

West, E.L., Pearson, R.A., Tschernutter, M., Sowden, J.C., MacLaren, R.E., and Ali, R.R. (2008). Pharmacological disruption of the outer limiting membrane leads to increased retinal integration of transplanted photoreceptor precursors. Exp. Eye Res. *86*, 601–611.

Wu, S., Chang, K.C., Nahmou, M., and Goldberg, J.L. (2018). Induced pluripotent stem cells promote retinal ganglion cell survival after transplant. Invest. Ophthalmol. Vis. Sci. *59*, 1571–1576.

Yamagata, M., and Sanes, J.R. (2008). Dscam and Sidekick proteins direct lamina-specific synaptic connections in vertebrate retina. Nature *451*, 465–469.

Yamagata, M., and Sanes, J.R. (2012). Expanding the Ig superfamily code for laminar specificity in retina: expression and role of contactins. J. Neurosci. *32*, 14402–14414.

Yin, Y.Q., Henzl, M.T., Lorber, B., Nakazawa, T., Thomas, T.T., Jiang, F., Langer, R., and Benowitz, L.I. (2006). Oncomodulin is a macrophage-derived signal for axon regeneration in retinal ganglion cells. Nat. Neurosci. *9*, 843–852.

Young, M.J., Ray, J., Whiteley, S.J., Klassen, H., and Gage, F.H. (2000). Neuronal differentiation and morphological integration of hippocampal progenitor cells transplanted to the retina of immature and mature dystrophic rats. Mol. Cell Neurosci. *16*, 197–205.

Zhang, X., Tenerelli, K., Wu, S., Xia, X., Yokota, S., Sun, C., Galvao, J., Venugopalan, P., Li, C., Madaan, A., et al. (2020). Cell transplantation of retinal ganglion cells derived from hESCs. Restor Neurol. Neurosci. *38*, 131–140.

Zou, T., Gao, L., Zeng, Y., Li, Q., Li, Y., Chen, S., Hu, X., Chen, X., Fu, C., Xu, H., et al. (2019). Organoid-derived C-Kit(+)/SSEA4(-) human retinal progenitor cells promote a protective retinal microenvironment during transplantation in rodents. Nat. Commun. *10*, 1205.